Published in final edited form as:
Dev Biol. 2009 March 15; 327(2): 327. doi:10.1016/j.ydbio.2008.12.009.

Morphogenetic movements driving neural tube closure in *Xenopus* require myosin IIB

Ana Rolo[*,‡], **Paul Skoglund**, and **Ray Keller**
Department of Biology, University of Virginia, Charlottesville, VA 22903, USA

Abstract

Vertebrate neural tube formation involves two distinct morphogenetic events -convergent extension (CE) driven by medio-lateral cell intercalation, and bending of the neural plate driven largely by cellular apical constriction. However, the cellular and molecular biomechanics of these processes are not understood. Here, using tissue-targeting techniques, we show that the myosin IIB motor protein complex is essential for both these processes, as well as for conferring resistance to deformation to the neural plate tissue. We show that myosin IIB is required for actin-cytoskeletal organization in both superficial and deep layers of the *Xenopus* neural plate. In the superficial layer, myosin IIB is needed for apical actin accumulation, which underlies constriction of the neurepithelial cells, and that ultimately drive neural plate bending, whereas in the deep neural cells myosin IIB organizes a cortical actin cytoskeleton, which we describe for the first time, and that is necessary for both normal neural cell cortical tension and shape and for autonomous CE of the neural tissue. We also show that myosin IIB is required for resistance to deformation ('stiffness') in the neural plate, indicating that the cytoskeleton-organizing roles of this protein translate in regulation of the biomechanical properties of the neural plate at the tissue-level.

Keywords

Myosin IIB; Xenopus; morphogenesis; convergent extension; neural plate; neural tube closure; actin; elastimeter

INTRODUCTION

The vertebrate neural tube forms from an initially flat, short and broad neural plate which then undergoes dramatic morphogenetic events that not only bend and roll it into a tube, but also greatly narrow and lengthen it along its antero-posterior axis (Jacobson and Gordon, 1976; Schoenwolf and Smith, 1990). This narrowing and lengthening of the neural tissue, commonly referred to as convergent extension (CE), is important for neural tube closure, as it brings the neural folds toward the midline, where they will meet and fuse (Wallingford and Harland, 2002). In a urodele (tailed) amphibian, *Taricha torosus*, neural CE is largely dependent on CE of the underlying dorsal mesoderm (Jacobson and Gordon, 1976). The anuran (tailless) amphibian *Xenopus laevis*, however, shows a form of neural CE that is mechanically independent of the underlying mesoderm (Elul et al., 1997; Keller and Danilchik, 1988; Keller

*Corresponding author: a.rolo@ucl.ac.uk.
‡Present address: Cell and Developmental Biology, University College London, Gower Street, London, WC1E 6BT, UK

et al., 1992a; Keller et al., 1992b). In sandwich explants, this mode of neural CE is induced and maintained by planar organizer signals without continued vertical signaling from the underlying mesoderm (Keller et al., 1992b). In isolated deep neural plate explants, it occurs by mediolateral cell intercalation of the deep mesenchymal cells of the double layered *Xenopus* neural plate, using a bipolar protrusive activity like that seen in the intercalating presumptive mesodermal cells (Elul et al., 1997). In contrast, with normal, continued vertical interactions with the underlying mesoderm, this bipolar mode is replaced with a monopolar, medially directed protrusive activity that is more efficient in producing neural cell intercalation and CE (Elul and Keller, 2000; Ezin et al., 2003). This medially-directed protrusive activity is dependent on unknown signals emanating from the midline tissues of notochord and the overlying notoplate (Ezin et al., 2003; Ezin et al., 2006). CE of the neural plate, like that of the dorsal mesoderm, is dependent on the vertebrate non-canonical Wnt/planar cell polarity (PCP) pathway (Wallingford and Harland, 2001; Wallingford and Harland, 2002). However, the mechanism by which the neural cells are polarized, how they produce the forces that drive their intercalation, and the relative contribution of the autonomous neural CE movements to the forces that shape the neural plate and roll it into a tube remain unresolved.

Medial movement of the neural folds involves bending of the neural plate. This process is driven largely by shape changes in neuroepithelial cells, which undergo apical constriction and assume a wedge or bottle-cell morphology, thus causing the neural sheet to bend (Burnside and Jacobson, 1968; Schoenwolf and Smith, 1990). The actin-binding protein Shroom is a key regulator of apical constriction during *Xenopus* anterior neural tube closure (Haigo et al., 2003), and in cultured MDCK cells, Shroom causes apical constriction by regulating the apical positioning of a contractile actomyosin network (Hildebrand, 2005).

Myosin II is a motor protein that binds to actin filaments and moves along them by hydrolyzing ATP, and also serves as an actin cross-linker (Laevsky and Knecht, 2003; Xu et al., 2001). Vertebrates have at least two genes encoding two different non-muscle myosin II heavy chain proteins - MHC-A, MHC-B (Katsuragawa et al., 1989; Kawamoto and Adelstein, 1991; Kelley et al., 1995). A third isoform, MHC-C, has been identified in mouse (Golomb et al., 2004). MHC-A is the predominant isoform expressed in *Xenopus* early embryonic cells (Kelley et al., 1996), but MHC-B is up-regulated in dorsal tissues that undergo CE (Bhatia-Dey et al., 1998) and myosin IIB is necessary for CE of the dorsal axial and paraxial mesoderm and blastopore closure in *Xenopus* (Skoglund et al., 2008). Myosins IIA and IIB have distinct biochemical properties, with IIB having a higher duty ratio, consistent with a role in maintaining cortical tension by cross-linking the cortical actin cytoskeleton (Kovacs et al., 2003; Rosenfeld et al., 2003; Wang et al., 2003). In the mouse, MHC-B plays an important role in neural development, particularly in the migration of certain groups of neurons (Ma et al., 2004; Ma et al., 2006; Tullio et al., 2001), and also in growth cone extension (Bridgman et al., 2001; Brown and Bridgman, 2003).

Here we examine the role of myosin IIB in *Xenopus* neural tube closure. We show that MHC-B is expressed in *Xenopus* neural tissues throughout neurulation, and that its partial knockdown causes delayed and defective neural tube closure, due to impairment of both CE and bending of the neural plate, as well as a general increase in deformability at the tissue-level. Neural plate superficial cells that normally drive bending of the neural plate by apical constriction, concomitant with apical actin accumulation, fail to do so when depleted of myosin IIB, whereas analysis of neural deep cells depleted of myosin IIB during the process of neural CE reveals defects in cell shape and cortical actin cytoskeletal integrity that are consistent with reduced cortical tension and changes in biomechanical properties of the cells. Defects in mechanical properties at tissue level are revealed by measurements of deformability of neural plates depleted of myosin IIB.

MATERIALS AND METHODS

Embryos and microsurgery

Xenopus laevis embryos were obtained and dejellied by standard methods (Sive et al., 2000) and staged according to Nieuwkoop and Faber (1994). Keller sandwiches were made from ~100° of the dorsal marginal zone according to Keller and Danilchik (1988) and neural-deep-over-mesoderm explants were made according to Elul and Keller (2000).

Whole-mount immunofluorescence

Albino embryos or explants were fixed in Dent's fixative (4:1 methanol:DMSO) for 2 hours at room temperature and stored at −20°C for an overnight period or longer. Whole embryos were bisected transversely with a scalpel after re-hydration, prior to immunostaining. MHC-B was detected using a polyclonal isoform-specific primary antibody (Covance, Berkeley, CA) at 1:50 dilution and a rhodamine-conjugated goat anti-rabbit secondary antibody (Jackson Immuno Research, West Grove, PA) at 1:200. Fibronectin was detected using a monoclonal primary antibody (4H2) (Davidson et al., 2004) at 1:200 dilution and an Alexa488-conjugated goat anti-mouse secondary antibody (Invitrogen - Molecular Probes, Carlsbad, CA) at 1:500. Embryos and explants were dehydrated in methanol and cleared in 2:1 benzyl benzoate:benzyl alcohol. Confocal images were collected using a BioRad Radiance 2100 and processed using ImageJ software.

Morpholino oligonucleotide and rescues

A previously described MO against the start site of MHC-B was used (CTTCCTGCCCTGGTCTCTGTACAT), as well as a control MO (CoMO) that varies at five nucleotides (CTTgCTcCCCTGcTCTCTcTAgAT) (Skoglund et al., 2008). 2-cell stage embryos were injected with 5 pmol of MO per blastomere to obtain a final MO concentration of 10μM. 8-cell stage embryos were injected with 0.312 pmol of MO per blastomere to obtain final MO concentration of 2.5μM. 32-cell stage embryos were injected with 0.125 or 0.156 pmol of MHC-B MO per blastomere to obtain final MO concentrations of 2 and 2.5 μM, respectively. Rescue experiments were done with a human MHC-B- GFP fusion DNA construct (Vicente-Manzanares et al., 2007), targeted to the neural plate by injecting 12.5 pg/embryo at the 8-cell stage.

In situ hybridization

In situ hybridizations were made according to Harland (1991) with probes against N-CAM (Kintner and Melton, 1987), N-β-tubulin (Chitnis et al., 1995), Slug (Mayor et al., 1995) and Rx1 (Casarosa et al., 1997).

Phalloidin staining

Embryos were transversely sectioned with a scalpel blade before staining with Rhodamine-conjugated phalloidin (Invitrogen - Molecular Probes, Carlsbad, CA) according to Haigo et al. (2003) and mounted in 1:1 glycerol:PBS. Confocal images were collected using a BioRad Radiance2100 and processed using ImageJ software.

Live cell imaging

Neural deep cells were imaged in neural-deep-over-mesoderm explants made from embryos injected at 2-cell stage with 50 or 200 pg per blastomere of the membrane targeted fluorophores pCS2+/GAP43-GFP or pCS2+/GAP43-RFP (Stubbs et al., 2006), respectively, and at the 32-cell stage with 12.5 pg per blastomere of pCSnucGFP (nuclear targeted GFP) (Kroll and Amaya, 1996) or with 50 pg per blastomere CS107-GFP-Moe (F-actin binding) (Litman et al., 2000), with or without MHC-B MO. Confocal live images were collected using a BioRad

Radiance2100 and processed using ImageJ software. F-actin imaging was done <2μm deep in the cell cortex using a 60x oil lens with a numerical aperture of 1.4.

Measurement of tissue deformability

The negative pressure needed to pull neural plate tissue into a pipette to the depth of the diameter of the bore of the microcap (about 280 mm) was measured using an apparatus and protocol similar to that used by Mitchison and Swann (1954) and Tickle and Trinkaus (1973). Four microliter Drummond Microcap tubes (Drummond Scientific Company, Broomall, PA), controlled by a micromanipulator, were used. Their broad, flat and smooth surfaces seal well against embryonic tissue. The tube was connected by flexible polyethylene tubing to a U-shaped, 8 mm diameter clear flexible tube about 1 m long, with each limb of the "U" fastened to two boards mounted on roller bearing drawer slides. The bottom third of the "U" was filled with dyed water, laced with a small amount of dish soap. Negative pressure was generated by rotating a dial, which moved one slide up and the other down, and the pressure was measured as the difference in height (in cm) of the level of water in the two limbs of the loop; a vent valve between the measuring loop and the microcap tubing allowed quick "zeroing" (equalization of the water levels). Measurements were done by placing embryos in a shallow pool of media confined to the bottom of an upside-down 60 mm culture dish rimmed with high vacuum silicone, and orienting them with a forceps between a back stop (the edge of a microscope slide glued to dish) and the microcap tube; the microcap tube, which has a polished flat surface, was pushed against the surface in the appropriate region of the neural plate and the dial turned slightly to raise the near limb of the loop relative to the far limb, generating a negative pressure; if the surface of the neural immediately deformed slightly, a seal had formed; if not, the microcap was rocked back and forth a bit to establish a seal. When a seal formed, the dial was rotated continuously until a protrusion of the neural plate was pulled into the microcap to the depth of the microcap diameter (determined with an ocular micrometer) (about 3–5 seconds), and the difference in level of water in the tubes measured in cm. After the pull, the dial was rotated in the opposite direction, and a positive pressure generated to expel the protrusion. To assure MO and mRNA injected regions were being tested, these reagents were co-injected with fluorescent dextran and the pulls were targeted to regions showing fluorescence.

Xdd1 and GFP mRNA injections

Xdd1 mRNA (Sokol, 1996) and GFP mRNA were injected at the 8-cell stage at 250pg per blastomere, together with 700pg of Alexa555-dextran (Invitrogen - Molecular Probes, Carlsbad, CA).

RESULTS

Myosin IIB is expressed in the neural plate of *Xenopus*

Immunostaining of the early neurula with an MHC-B specific antibody shows MHC-B in the basal ends of the deep cells of the neural plate, as well as in other dorsal tissues, particularly in the presumptive notochord (Fig. 1A). By neural fold stages, MHC-B staining is strong in both layers of the neural plate, with the basal surface of the deep layer remaining the most strongly stained, and it has a clear cortical sub-cellular localization (Fig. 1B). In the tailbud stages there is particularly strong staining in the basal (outer) ends of the neural tube cells, as well as in the neural crest region (Fig. 1C). MHC-B is high in the basal epidermis (Fig. 1C) and in scattered cells of the outer epidermis (Fig. 1C, asterisks) that correspond to epidermal ciliated cells (data not shown). In addition, we confirm strong expression in the notochordal and somitic mesoderm at these stages (Skoglund et al., 2008) (Fig. 1C).

The MHC-B at tissue boundaries appears to coincide with the extracellular matrix, particularly with fibrillar fibronectin (Davidson et al., 2004; Goto et al., 2005). Co-staining of MHC-B and fibronectin confirmed localization of fibronectin to tissue boundaries (Fig. 1D) and co-localization of the two proteins in the outer basal surface of the neural tube, around the neural crest, around the notochord, and in the basal epidermis (Fig. 1E). For a higher resolution, we immuno-stained neural-deep-over-mesoderm explants (Elul and Keller, 2000), which lack epithelial tissues and therefore allow better antibody penetration. As in whole embryos, fibronectin and MHC-B are co-localized to the boundaries between the notochordal and somitic tissues and at the basal surface of the neural plate in these explants (Fig. 1F–H). *En face* images of the interface of the neural plate and dorsal mesoderm show MHC-B in a fibrillar pattern (Fig. 1I) that overlaps the fibronectin fibrils (Fig. 1J, K). Staining for MHC-B alone (not shown) showed a pattern similar to that seen in the co-labeling experiment (Fig. 1F, I), therefore ruling out the possibility that the overlap between fibronectin and MHC-B staining was due to spectral bleed-through. This result is consistent with myosin IIB having an essential role in cell-fibronectin adhesion, as we have previously described (Skoglund et al., 2008).

Effectiveness and specificity of MHC-B morpholino

A knock-down of myosin IIB in neural morphogenesis was done with a morpholino oligonucleotide (MO) against MHC-B, which causes gastrulation and mesodermal CE defects in whole embryos (Skoglund et al., 2008). Here we confirm the effectiveness and specificity of the MHC-B MO, previously shown by Western blot analysis (Skoglund et al., 2008), by whole-mount immunostaining of embryos injected in one cell at the 2-cell stage with either MHC-B MO or a control MO (CoMO, see Materials and Methods). The embryos injected with CoMO show no reduction of MHC-B protein levels (Fig. 1L), whereas embryos injected with MHC-B MO present a clear reduction of MHC-B on the injected side (Fig. 1M).

To minimize effects on the mesoderm in the experiments presented here, the MO was targeted to the entire neural plate by injecting dorsal (A- and B-tier) animal blastomeres of the 8-cell stage embryos that were selected for regular cleavage patterns and for third cleavage planes located relatively near the animal pole. The MHC-B MO and CoMO were injected to a final concentration of 2.5μM, at which the MHC-B MO causes a mild gastrulation phenotype in whole embryos (Skoglund et al., 2008). Targeting was evaluated by coinjecting a fluorescent dye together with the MO, and the criteria for successful cases were stage 12.5 embryos that showed fluorescence in all or most of the neural plate region (Fig. 2A, t=0h) and showed blastopore closure similar to control embryos (Fig. 2A, t=0h), indicating no effect of the MO on the dorsal mesoderm. The MHC-B MO did not affect neural cell fates as shown by absence of changes in expression of pan-neural, neuronal, neural crest or prospective eye markers (Fig. S1).

MHC-B MO targeted to the neural plate causes delayed and defective neural tube closure

Time-lapse video-recordings of neurulation in un-injected embryos and in neural targeted CoMO and MHC-B MO embryos (Fig. 2A) revealed a delay in neural tube closure in morphant embryos, and this delay was more pronounced in anterior regions. At stage 19, when all un-injected embryos had fully closed neural tubes (22/22), only 15% (6/40) of MHC-B morphants had closed their neural tubes, whereas more than 85% (18/21) of CoMO embryos had successfully achieved this stage. At control stage 17–18, areas of darker pigmentation, which correspond to apical constriction of cells that function in closing the brain region of the neural plate, appear in un-injected embryos (arrows, Fig. 2A, t=3h and 4h), and the same are apparent slightly later in CoMO embryos (arrows, Fig. 2A, t=5h), but these are never observed in MHC-B morphant embryos. Later, at tailbud stages, most MHC-B morphants displayed moderate to severe dorsal flexure (37/39, Fig. 2C), whereas this phenotype was only rarely observed in CoMO injected embryos (3/21, Fig. 2B).

Myosin IIB reduction causes defects in apical actin accumulation and apical constriction in neural plate superficial cells

When MHC-B MO was targeted to the neural plate unilaterally, the anterior neural fold on the morphant side did not rise as prominently (right side, Fig. 3A), and it converged medially more slowly than its counterpart on the un-injected side (left side, Fig. 3A). Apical F-actin accumulation, which accompanies apical constriction and bottle cell formation (Haigo et al., 2003), did not occur on the morphant side, whereas it did on the uninjected side (6/6) (Fig. 3B), suggesting that apical constriction failed on the morphant side. Cross-sections through the brain and spinal cord regions of stage 17–18 embryos confirm that morphant cells did not constrict their apices nor adopt the normal bottle-cell shape (1/48 bottle-shaped cells in 6 sections) (red cells, right, Fig. 3C-C′ and D-D′), compared with the elongated bottle-cell shape and very narrow apices of normal neural epithelial cells (43/60 bottle-shaped cells in 6 sections) (left side, Fig. 3C-C′, D-D′).

MHC-B MO effects on autonomous neural CE

The dorsal flexure observed following MHC-B reduction (Fig. 2C) could result from defective neural CE. In Keller explants, both neural and mesodermal tissues undergo active, mechanically independent CE (Keller and Danilchik, 1988), but in whole embryos, the extension of the neural tissue occurs in parallel to and is mechanically coupled to the extension of the underlying mesodermal tissues, particularly during neurulation (Keller et al., 1992b). In tailbud stages, both these dorsal tissues may be mechanically coupled to the ventral part of the embryo, which also extends at these stages, causing a straightening of the trunk in anurans (Larkin and Danilchik, 1999) and in urodeles (Drawbridge and Steinberg, 2000). Thus failure of neural extension, mesodermal extension, or both, could slow extension of the dorsal side relative to the ventral side, and thus result in dorsal flexure. Therefore, one cannot rule out the possibility that the arched phenotype is partly due to presence of MHC-B MO in mesodermal tissues.

To address this issue, the effect of MHC-B depletion on neural CE was assayed in Keller sandwiches, which comprise the dorsal sector of the gastrula explanted and sandwiched together at early gastrula stages, such that the neural and mesodermal tissues extend serially, in opposite directions, and mechanically independent of one another (Keller and Danilchik, 1988) (Fig. 4A). Neural extension in explants in which MHC-B MO was targeted to the presumptive neural region (Fig. 4B) was less than the extension in control explants (Fig. 4A) by more than two-fold (Fig. 4C). The mesodermal extension in morphant explants was slightly less than in control explants (Fig. 4C), a reduction that can be explained by the presence of some MO in the posterior part of the mesoderm, which is seen by the presence of the fluorescent dye co-injected with the MO (Fig. 4B′). Considering individual cases, the reduction of mesodermal extension correlates with the amount of MO found in the mesoderm. For example, the two explants on the right (Fig. 4B) show higher fluorescence in the mesoderm and also decreased extension of this tissue, when compared to the three explants on the left, all of which have less fluorescence in the mesoderm and also greater mesodermal extension.

To assess the specificity of the neural CE impairment caused by the MHC-B MO, we expressed human MHC-B (Vicente-Manzanares et al., 2007) (which varies by 17 of 25 nucleotides over the region targeted by the frog MHC-B MO) fused with GFP in the neural plate, together with the MHC-B MO, as above. This combination produced a partial rescue (28%) of neural extension in Keller sandwiches (Fig. 4D), thus confirming that the impairment in neural CE is due to reduced levels of myosin IIB. The partial nature of this rescue may be due to differences in timing, patterning, or levels of expression of the exogenous human MHC-B as compared to that normally exhibited by *Xenopus* MHC-B, or because inherent differences between human and *Xenopus* MHC-B′s lead to sub-optimal functioning of the cortical actin network during

morphogenesis when these proteins are substituted, similar to the partial developmental rescue obtained in mice engineered to replace MHC-B with MHC-A under the control of the MHC-B promoter (Bao et al., 2007).

These results show that myosin IIB is essential for mechanically independent neural CE.

MHC-B reduction causes defects in cell motility, cell shape, and the actin cytoskeleton of neural plate deep cells

To analyze the cellular basis of the impaired neural CE in morphant embryos, the MHC-B MO was targeted to scattered cells in the neural plate by dorsal injection at the 32 or 64-cell stage. Normal cells show sharply defined filiform and lamelliform protrusions with the normal concave marginal profile between protrusions (Fig. 5A). The cortical actin cytoskeleton, visualized using the F-actin binding GFP probe CS107-GFP-Moe, formed a well-organized network of actin bundles radiating from one or more foci within the cell. This actin array contracts episodically in conjunction with contractions of the cell body (31/31 – 100% of cells in 8 explants) (Fig. 5A and Supplementary Movie 1). At 2μM MO, the cells are hyper-elongated and the actin bundles do not connect at foci but rather form long straight cables parallel to the direction of cell elongation, that still contract episodically (9/12 – 75% of cells in 2 explants) (Fig. 5B and Supplementary Movie 2). At 2.5μM MO, the cells are misshapen, flatter, occupy a larger area in the plane of the neural plate, and show abnormal protrusive activity (27/27 – 100% of cells in 4 explants) (Fig. 5C, D, and Supplementary Movie 3). They form large, blunt protrusions, sometimes with multiple lobes, and with convex profiles where they meet the cell body (cf. Fig. 5A, C–D). They also have sparser, coarser cortical actin network consisting of fewer but thicker cables that are curved and rarely straight for any length (Fig. 5C). These cables flow in the same direction of cell movement, which occurs without apparent episodic contractions of either the cell body or the cytoskeleton (Fig. 5C and Supplementary Movie 3). In some cases, actin bundles are almost absent (Fig. 5D). In addition, the morphant cells have yolk granules present in the cortex, as shown by exclusion of GFP fluorescence (asterisks, Fig. 5C, D), whereas in control cells yolk granules are excluded from the cortex (Fig. 5A), and can only be found starting at ~5 μm into the cytoplasm (not shown), similar to dorsal mesodermal cells (Skoglund et al., 2008). Eventually, most of these cells are extruded from the tissue (Fig. 5C–D), presumably from loss of cell-cell and cell-matrix adhesion, also similar to what happens with morphant mesodermal cells (Skoglund et al., 2008).

The above observations suggest that the morphant cells have a dose-dependent, progressively reduced control of the mechanical properties of their cortical region. At 2μM MO, the cells maintain their adhesion and thus tissue remains mechanically intact, and they also show their characteristic mediolateral elongation. But compared to control cells (Fig. 5E), which have an average length-to-width ratio of 1.69 ± 0.08 (n=43), the morphant cells attain a significantly greater average length-to-width ratio of 2.74 ± 0.13 (n=43) (Fig. 5F), suggesting that the morphant cells have less ability to resist mediolateral tensile forces in the intact neural plate. These elongated morphant cells regularly round up and undergo mitosis and cytokinesis (Fig. 5G), which shows that 2μM MHC-B MO does not affect cytokinesis, and is consistent with findings in *Drosophila* that the cell rounding and increased cortex rigidity upon entry into mitosis are myosin II-independent, relying instead on the actin-binding protein Moesin (Kunda et al., 2008).

Myosin IIB depletion increases the deformability of the neural tissue

The excessive medio-lateral cell elongation, the appearance of the cytoskeleton, and the retarded rate of moving the neural folds medially and upward toward one another in myosin IIB depleted embryos suggest that the cortical actin cytoskeleton, and therefore the cells, and neural plate tissue, are more deformable and thus cannot generate the tensile forces necessary

to move the tissue toward the midline. To test this possibility, we determined the negative pressure necessary to pull neural plate tissue into a pipette to a standard depth of one capillary diameter (see Materials and Methods) (Tickle and Trinkaus, 1973; Mitichison and Swann, 1954) (Fig. 6). The standard size of the pulled protrusion was determined because shorter pulls (pulling a hemispherical dome, the depth of the capillary radius) involved mostly bending of the neural plate surface, whereas the longer, diameter-length pull involved considerable tissue stretching and cell shape change, the parameter of most interest, but little cell neighbor change, as observed with the stereoscope. Also, the epithelial layer of the pulled protrusion rarely broke open in uninjected and CoMO injected tissue, whereas it often broke open in MHC-B depleted embryos (not shown).

Neural plates of control (un-injected) embryos showed a large increase in stiffness (decreased deformability) from stage 10.5–11 to stage 11.5, and slowly increased stiffness through neurulation (Fig. 6). MHC-B MO (2.5 μM dose) injected neural plates show dramatically decreased stiffness (increased deformability) of almost half the normal stiffness during the period of rapid narrowing of the neural plate (stage 12.5–16), whereas control MO (CoMO) embryos have unchanged stiffness (Fig. 6).

To determine whether the increased deformability following MHC-B depletion is characteristic of other perturbations that produce neural convergent extension and neural tube closure defects, we injected mRNA encoding a dominant negative disheveled (Xdd1), which inhibits the non-canonical Wnt/vertebrate planar cell polarity pathway essential for convergent extension and neural tube closure (see Sokol, 1996; Wallingford et al., 2000; Wallingford and Harland, 2001; Wallingford and Harland, 2002), targeted to the neural plate at a concentration of 250pg per blastomere (500pg total), which consistently lead to defects in neural tube closure (not shown) (Wallingford and Harland, 2001; Wallingford and Harland, 2002). We compared the deformability of these neural plates with those injected with mRNA encoding GFP and uninjected embryos (Fig. 6). No statistically significant difference was found, showing that the increased deformability of the neural plate was a specific defect caused by myosin IIB depletion, rather than a general defect underlying all types of neural CE perturbations.

DISCUSSION

We show that myosin IIB is expressed in the *Xenopus* neural plate and neural tube, and that it is required in these tissues for apical constriction and CE movements that drive neural tube closure, as well as for stiffness of the neural tissues. Apical constriction of neural superficial cells is presumably dependent on apical accumulation of actin, and myosin IIB is required for both these events. Myosin IIB is also required in the neural deep layer of cells for autonomous neural CE and its depletion leads to disruption of the cortical actin cytoskeleton, abnormal cell shape and abnormal protrusive activity; these defects manifest themselves at the tissue-level by an increase in deformability of the neural plate. These findings parallel the analysis of myosin IIB in mesodermal CE, which showed that MHC-B reduction in dorsal mesoderm cells leads to similar changes in cytoskeletal organization, cell shape, cell protrusive activity, and cell-cell and cell-matrix adhesion (Skoglund et al., 2008), and they reveal both similar and novel roles for myosin IIB in neural morphogenesis.

Myosin IIB has multiple roles of varying sensitivity

We have shown that neural depletion of MHC-B causes distinct defects in the two layers of the *Xenopus* neural plate, suggesting that this protein has different cell biological roles in neurulation. This suggestion is supported by the fact that myosin II has several distinct cellular functions in other systems, such as regulation of cell shape and cortical integrity (Egelhoff et al., 1996; Laevsky and Knecht, 2003; Xu et al., 2001), cell motility (Bridgman et al., 2001; Gupton et al., 2005; Lo et al., 2004; Svitkina et al., 1997), and cell adhesion (Shewan et al.,

2005). The observation that high levels of MHC-B MO result in exclusion of neural cells from the neural plate shows that myosin IIB is essential for neural cell adhesion and tissue integrity, just as it is necessary for cell-cell and cell-matrix adhesion during CE of the dorsal mesoderm (Skoglund et al., 2008). In cultured mammalian epithelial cells, myosin II is essential for concentration of E-cadherin at cell junctions during cell adhesion (Shewan et al., 2005). Myosin IIB may play a similar role in clustering of the cadherins shown to function during neurulation, N-cadherin and F-cadherin (Detrick et al., 1990; Espeseth et al., 1995). At the lower MHC-B MO levels used for most of the analysis here, loss of adhesion does not occur, and neural tissue integrity is maintained, probably because the myosin IIB remaining at these doses is sufficient for cell adhesion. This partial depletion of myosin IIB in neural tissues reveals additional defects that correspond to other roles of this protein in neurulation, which are more sensitive to reduction of protein levels than cell adhesion.

Myosin IIB function plays a role in both the deep and superficial neural plate layers

A delay in neural tube closure can be caused by different factors. Defects in neural CE, which is an active process driven by the deep layer of the neural plate in *Xenopus* (Elul et al., 1997; Keller and Danilchik, 1988; Keller et al., 1992a), cause the neural plate to be wider than normal and thus the neural folds may not meet and fuse to form a tube (Wallingford and Harland, 2002). But the anterior region of the neural plate where the delay is greatest does not show as much CE or mediolateral cell intercalation as the posterior regions (Keller et al., 1992a). Therefore most of the anterior delay in morphant embryos is probably due to failure of bending of the neural plate such that the neural folds are brought medially, an interpretation supported by our observation that myosin IIB depletion results in reduced apical constriction, reduced cell wedging, and slower bending of the superficial, epithelial layer of the neural plate, all processes that are important in neural tube closure (Burnside and Jacobson, 1968; Haigo et al., 2003; Jacobson and Gordon, 1976; Schoenwolf and Smith, 1990).

Nevertheless, when autonomous neural CE was assayed by mechanically separating it from mesoderm CE using the Keller sandwich explant, there was a strong dependence on myosin IIB. In *Xenopus*, mesodermal CE is stronger than the neural CE, judging from the fact that when the mesodermal and neural extensions are placed in apposition to one another in mechanically confined Keller explants, it is the neural regions that fails to extend or buckles under the compressive force developed by the mesodermal region (R. Keller, unpublished observations; see Moore, 1992). Thus in *Xenopus*, where CE of the underlying mesoderm is strong enough to stretch the overlying attached neural tissue, depletion of myosin IIB in neural tissue has a relatively weak phenotype due to ‘towing’ by the mesoderm, which is presumably facilitated in morphant embryos due to their increased deformability. However, myosin IIB may have a much larger role in other vertebrates in which neural CE may play a relatively larger role, perhaps even larger than mesodermal CE, in axis extension.

Myosin IIB regulates mechanical properties of the neural plate at cellular and tissue levels during CE

Dictyostelium cells lacking myosin II have defects in cell shape and motility, and in this case, it was shown that myosin II regulates cortical integrity and cortical tension by serving as the major actin cross-linker of the cell, with this activity being more relevant than its motor function (Egelhoff et al., 1996; Laevsky and Knecht, 2003; Xu et al., 2001). Interestingly, myosin IIB, when compared to myosin IIA, has an extended duty cycle and a slow rate of translocation on actin filaments, properties that are more consistent with it serving primarily as a cross-linker than as a motor in producing actin filament movement (Rosenfeld et al., 2003; Wang et al., 2003).

Our results argue that myosin IIB may serve first and foremost as an actin filament cross-linker that is necessary for maintaining cortical integrity and stiffness. This model is consistent with the progressive effect of increasing doses of MHC-B MO on the cortical actin network and on the cell morphologies. At low MO concentrations, the cells remain adhesive and tissue integrity is preserved, and thus the mediolaterally-oriented, tractional forces thought to bring about convergence would have to be borne by the individual cells, whether that traction was on other cells or the attached extracellular matrix. Since at low MO levels, the morphant cells also maintain their elongated, oriented shape and polarized protrusive activity, and we believe that this protrusive activity puts the cell under mediolateral tension, though perhaps not as much as in the normal case, and that this tension elongates the individual cells abnormally in the face of their weaker cortical actin cytoskeleton and thus weaker resistance to mechanical stretching. This hypothesis is consistent with the hyper-elongation of morphant neural cells that we observe, and with fact that myosin IIB depleted cells cultured on traction-measuring substrates do develop traction forces (Lo et al., 2004). The loss of polarity we see at a higher MO level is also consistent with observations in cultured fibroblasts that myosin II regulates protrusive activity and stabilizes cell polarity (Lo et al., 2004). Loss of adhesion at higher levels of MO also disrupts tissue integrity and thus the cells are not exposed to tissue-level tensile forces. These observations suggest that myosin IIB has roles in cortical integrity, polarized cell motility, and cell adhesion, and that these roles are progressively less sensitive in this order to reduced MHC-B levels. Although we believe an actin cross-linking role is sufficient to account for our observations, a contractile role for myosin IIB is not ruled out by our experiments, because we do not know whether the cytoskeleton provides a passive resistance to stretching or whether it actively resists stretching by contraction in its role of limiting the elongation of the neural cells discussed here, or the mesodermal cells (Skoglund et al., 2008). The apparent decrease in resistance to stretching on MHC-B depletion could be due to weakening of an active, myosin IIB mediated contraction of the cortical actin meshwork, or it could reflect a decreased cross-linking of the actin network, making it easier to stretch in either case.

The cytoskeletal disruptions caused by MHC-B depletion and consequent changes in cortical stiffness are also evident at the tissue level. MHC-B morphant neural plates are mechanically more pliable and thus offer less mechanical resistance to being passively deformed. This may account for the fact that myosin IIB knockdown in neural plates of whole-embryos leads to a fairly slight dorsal flexure (because the morphant neural plate is passively elongated by the axial and paraxial mesoderm) in contrast to the strong inhibition of autonomous neural extension seen in sandwich explants. This contention is supported by the fact that when neural CE is blocked by perturbing the Wnt/PCP pathway, the dorsal flexure is much greater than the one caused here by myosin IIB perturbation (Wallingford and Harland, 2001; Wallingford and Harland, 2002). Furthermore, we show that Wnt/PCP perturbations, despite impairing neural CE, do not change the deformability of the neural plate, and thus in these cases the stiffer, non-extending neural plate resists passive stretching by CE of the mesoderm, thus resulting in severe dorsal flexure.

Towards understanding the molecular mechanisms of myosin II function in morphogenesis

The fact that progressively greater reduction of myosin IIB results in a dose-dependent sequence of phenotypes, beginning with apparent loss of cortical tension, loss of characteristic cell shape and polarized protrusive activity, and finally, at high levels of reduction, loss of cell-cell and cell matrix adhesion suggests that different cellular processes are differentially sensitive to myosin levels. Also, we show that myosin II functions in different processes, such as cell intercalation, a process regulated by the Wnt/PCP pathway (Wallingford and Harland, 2001; Wallingford and Harland, 2002), and also apical constriction of neuroepithelial cells, a process regulated by the Shroom protein and independent of Wnt/PCP (Haigo et al., 2003). Future challenges include learning how myosin II function is regulated by these different

pathways and what biochemical and mechanochemical properties of this molecule are relevant for each cell biological function.

Supplementary Material

Refer to Web version on PubMed Central for supplementary material.

Acknowledgments

We thank all the members in the Keller lab for stimulating discussions in the laboratory. We particularly thank Lance Davidson for imaging tips. We are also grateful to Ammasi Periasamy and Ye Chen for help with confocal imaging at the Keck Center for Cellular Imaging (KCCI) at the University of Virginia. The CS107-GFP-Moe plasmid was a kind gift from Dr. John Wallingford. We also thank Claudio Stern for allowing A. R. to finish the present work at his laboratory at UCL, Les Dale (UCL) for help with obtaining *Xenopus* embryos and Roberto Mayor (UCL) for access to time-lapse video-recording equipment. This work was supported by National Institutes of Health (NIH) grants HD36426-01 and HD25594-13 to R. K. and a predoctoral fellowship from Fundação para a Ciência e a Tecnologia (FCT) SFRH/BD/4851/2001 to A. R.

References

Bao J, Ma X, Liu C, Adelstein RS. Replacement of nonmuscle myosin II-B with II-A rescues brain but not cardiac defects in mice. J Biol Chem 2007;282:22102–11. [PubMed: 17519229]

Bhatia-Dey N, Taira M, Conti MA, Nooruddin H, Adelstein RS. Differential expression of non-muscle myosin heavy chain genes during Xenopus embryogenesis. Mech Dev 1998;78:33–6. [PubMed: 9858676]

Bridgman PC, Dave S, Asnes CF, Tullio AN, Adelstein RS. Myosin IIB is required for growth cone motility. J Neurosci 2001;21:6159–69. [PubMed: 11487639]

Brown ME, Bridgman PC. Retrograde flow rate is increased in growth cones from myosin IIB knockout mice. J Cell Sci 2003;116:1087–94. [PubMed: 12584251]

Burnside MB, Jacobson AG. Analysis of morphogenetic movements in the neural plate of the newt Taricha torosa. Dev Biol 1968;18:537–52. [PubMed: 5751536]

Casarosa S, Andreazzoli M, Simeone A, Barsacchi G. Xrx1, a novel Xenopus homeobox gene expressed during eye and pineal gland development. Mech Dev 1997;61:187–98. [PubMed: 9076688]

Chitnis A, Henrique D, Lewis J, Ish-Horowicz D, Kintner C. Primary neurogenesis in Xenopus embryos regulated by a homologue of the Drosophila neurogenic gene Delta. Nature 1995;375:761–6. [PubMed: 7596407]

Davidson LA, Keller R, DeSimone DW. Assembly and remodeling of the fibrillar fibronectin extracellular matrix during gastrulation and neurulation in Xenopus laevis. Dev Dyn 2004;231:888–95. [PubMed: 15517579]

Detrick RJ, Dickey D, Kintner CR. The effects of N-cadherin misexpression on morphogenesis in Xenopus embryos. Neuron 1990;4:493–506. [PubMed: 2322458]

Drawbridge J, Steinberg MS. Elongation of axolotl tailbud embryos requires GPI-linked proteins and organizer-induced, active, ventral trunk endoderm cell rearrangements. Dev Biol 2000;223:27–37. [PubMed: 10864458]

Egelhoff TT, Naismith TV, Brozovich FV. Myosin-based cortical tension in Dictyostelium resolved into heavy and light chain-regulated components. J Muscle Res Cell Motil 1996;17:269–74. [PubMed: 8793728]

Elul T, Keller R. Monopolar protrusive activity: a new morphogenic cell behavior in the neural plate dependent on vertical interactions with the mesoderm in Xenopus. Dev Biol 2000;224:3–19. [PubMed: 10898957]

Elul T, Koehl MA, Keller R. Cellular mechanism underlying neural convergent extension in Xenopus laevis embryos. Dev Biol 1997;191:243–58. [PubMed: 9398438]

Espeseth A, Johnson E, Kintner C. Xenopus F-cadherin, a novel member of the cadherin family of cell adhesion molecules, is expressed at boundaries in the neural tube. Mol Cell Neurosci 1995;6:199–211. [PubMed: 7496627]

Ezin AM, Skoglund P, Keller R. The midline (notochord and notoplate) patterns the cell motility underlying convergence and extension of the Xenopus neural plate. Dev Biol 2003;256:100–14. [PubMed: 12654295]

Ezin AM, Skoglund P, Keller R. The presumptive floor plate (notoplate) induces behaviors associated with convergent extension in medial but not lateral neural plate cells of Xenopus. Dev Biol 2006;300:670–86. [PubMed: 17034782]

Golomb E, Ma X, Jana SS, Preston YA, Kawamoto S, Shoham NG, Goldin E, Conti MA, Sellers JR, Adelstein RS. Identification and characterization of nonmuscle myosin II-C, a new member of the myosin II family. J Biol Chem 2004;279:2800–8. [PubMed: 14594953]

Goto T, Davidson L, Asashima M, Keller R. Planar cell polarity genes regulate polarized extracellular matrix deposition during frog gastrulation. Curr Biol 2005;15:787–93. [PubMed: 15854914]

Gupton SL, Anderson KL, Kole TP, Fischer RS, Ponti A, Hitchcock-DeGregori SE, Danuser G, Fowler VM, Wirtz D, Hanein D, Waterman-Storer CM. Cell migration without a lamellipodium: translation of actin dynamics into cell movement mediated by tropomyosin. J Cell Biol 2005;168:619–31. [PubMed: 15716379]

Haigo SL, Hildebrand JD, Harland RM, Wallingford JB. Shroom induces apical constriction and is required for hingepoint formation during neural tube closure. Curr Biol 2003;13:2125–37. [PubMed: 14680628]

Harland RM. In situ hybridization: an improved whole-mount method for Xenopus embryos. Methods Cell Biol 1991;36:685–95. [PubMed: 1811161]

Hildebrand JD. Shroom regulates epithelial cell shape via the apical positioning of an actomyosin network. J Cell Sci 2005;118:5191–203. [PubMed: 16249236]

Jacobson AG, Gordon R. Changes in the shape of the developing vertebrate nervous system analyzed experimentally, mathematically and by computer simulation. J Exp Zool 1976;197:191–246. [PubMed: 965908]

Katsuragawa Y, Yanagisawa M, Inoue A, Masaki T. Two distinct nonmuscle myosin-heavy-chain mRNAs are differentially expressed in various chicken tissues. Identification of a novel gene family of vertebrate non-sarcomeric myosin heavy chains. Eur J Biochem 1989;184:611–6. [PubMed: 2806244]

Kawamoto S, Adelstein RS. Chicken nonmuscle myosin heavy chains: differential expression of two mRNAs and evidence for two different polypeptides. J Cell Biol 1991;112:915–24. [PubMed: 1999462]

Keller R, Danilchik M. Regional expression, pattern and timing of convergence and extension during gastrulation of Xenopus laevis. Development 1988;103:193–209. [PubMed: 3197629]

Keller R, Shih J, Sater A. The cellular basis of the convergence and extension of the Xenopus neural plate. Dev Dyn 1992a;193:199–217. [PubMed: 1600240]

Keller R, Shih J, Sater AK, Moreno C. Planar induction of convergence and extension of the neural plate by the organizer of Xenopus. Dev Dyn 1992b;193:218–34. [PubMed: 1600241]

Kelley CA, Oberman F, Yisraeli JK, Adelstein RS. A Xenopus nonmuscle myosin heavy chain isoform is phosphorylated by cyclin-p34cdc2 kinase during meiosis. J Biol Chem 1995;270:1395–401. [PubMed: 7836406]

Kelley CA, Sellers JR, Gard DL, Bui D, Adelstein RS, Baines IC. Xenopus nonmuscle myosin heavy chain isoforms have different subcellular localizations and enzymatic activities. J Cell Biol 1996;134:675–87. [PubMed: 8707847]

Kintner CR, Melton DA. Expression of Xenopus N-CAM RNA in ectoderm is an early response to neural induction. Development 1987;99:311–25. [PubMed: 2443340]

Kovacs M, Wang F, Hu A, Zhang Y, Sellers JR. Functional divergence of human cytoplasmic myosin II: kinetic characterization of the non-muscle IIA isoform. J Biol Chem 2003;278:38132–40. [PubMed: 12847096]

Kroll KL, Amaya E. Transgenic Xenopus embryos from sperm nuclear transplantations reveal FGF signaling requirements during gastrulation. Development 1996;122:3173–83. [PubMed: 8898230]

Kunda P, Pelling AE, Liu T, Baum B. Moesin controls cortical rigidity, cell rounding, and spindle morphogenesis during mitosis. Curr Biol 2008;18:91–101. [PubMed: 18207738]

Laevsky G, Knecht DA. Cross-linking of actin filaments by myosin II is a major contributor to cortical integrity and cell motility in restrictive environments. J Cell Sci 2003;116:3761–70. [PubMed: 12890752]

Larkin K, Danilchik MV. Ventral cell rearrangements contribute to anterior-posterior axis lengthening between neurula and tailbud stages in Xenopus laevis. Dev Biol 1999;216:550–60. [PubMed: 10642792]

Litman P, Amieva MR, Furthmayr H. Imaging of dynamic changes of the actin cytoskeleton in microextensions of live NIH3T3 cells with a GFP fusion of the F-actin binding domain of moesin. BMC Cell Biol 2000;1:1. [PubMed: 11112983]

Lo CM, Buxton DB, Chua GC, Dembo M, Adelstein RS, Wang YL. Nonmuscle myosin IIb is involved in the guidance of fibroblast migration. Mol Biol Cell 2004;15:982–9. [PubMed: 14699073]

Ma X, Kawamoto S, Hara Y, Adelstein RS. A point mutation in the motor domain of nonmuscle myosin II-B impairs migration of distinct groups of neurons. Mol Biol Cell 2004;15:2568–79. [PubMed: 15034141]

Ma X, Kawamoto S, Uribe J, Adelstein RS. Function of the neuron-specific alternatively spliced isoforms of nonmuscle myosin II-B during mouse brain development. Mol Biol Cell 2006;17:2138–49. [PubMed: 16481398]

Mayor R, Morgan R, Sargent MG. Induction of the prospective neural crest of Xenopus. Development 1995;121:767–77. [PubMed: 7720581]

Mitchison JM, Swann MM. The mechanical properties of the cell surface. I. The cell elastimeter. J exp Biol 1954;31:443–461.

Moore, SW. Direct measurement of dynamic biomechanical properties of amphibian embryonic tissues. University of California at Berkeley; Berkeley, CA: 1992. p. 400

Nieuwkoop, PD.; Faber, J. Normal Table of Xenopus laevis (Daudin). Garland Publishing; New York: 1994.

Rosenfeld SS, Xing J, Chen LQ, Sweeney HL. Myosin IIb is unconventionally conventional. J Biol Chem 2003;278:27449–55. [PubMed: 12740390]

Schoenwolf GC, Smith JL. Mechanisms of neurulation: traditional viewpoint and recent advances. Development 1990;109:243–70. [PubMed: 2205465]

Shewan AM, Maddugoda M, Kraemer A, Stehbens SJ, Verma S, Kovacs EM, Yap AS. Myosin 2 is a key Rho kinase target necessary for the local concentration of E-cadherin at cell-cell contacts. Mol Biol Cell 2005;16:4531–42. [PubMed: 16030252]

Sive, HL.; Grainger, RM.; Harland, RM. Early Development of Xenopus laevis. Cold Spring Harbor Laboratory Press; Cold Spring Harbor, New York: 2000.

Skoglund P, Rolo A, Chen X, Gumbiner BM, Keller R. Convergence and extension at gastrulation require a myosin IIB-dependent cortical actin network. Development 2008;135:2435–44. [PubMed: 18550716]

Sokol SY. Analysis of Dishevelled signalling pathways during Xenopus development. Curr Biol 1996;6:1456–67. [PubMed: 8939601]

Stubbs JL, Davidson L, Keller R, Kintner C. Radial intercalation of ciliated cells during Xenopus skin development. Development 2006;133:2507–15. [PubMed: 16728476]

Svitkina TM, Verkhovsky AB, McQuade KM, Borisy GG. Analysis of the actin-myosin II system in fish epidermal keratocytes: mechanism of cell body translocation. J Cell Biol 1997;139:397–415. [PubMed: 9334344]

Tickle CA, Trinkaus JP. Change in surface extensibility of Fundulus deep cells during early development. J Cell Sci 1973;13:721–726. [PubMed: 4797866]

Tullio AN, Bridgman PC, Tresser NJ, Chan CC, Conti MA, Adelstein RS, Hara Y. Structural abnormalities develop in the brain after ablation of the gene encoding nonmuscle myosin II-B heavy chain. J Comp Neurol 2001;433:62–74. [PubMed: 11283949]

Vicente-Manzanares M, Zareno J, Whitmore L, Choi CK, Horwitz AF. Regulation of protrusion, adhesion dynamics, and polarity by myosins IIA and IIB in migrating cells. J Cell Biol 2007;176:573–80. [PubMed: 17312025]

Wallingford JB, Harland RM. Xenopus Dishevelled signaling regulates both neural and mesodermal convergent extension: parallel forces elongating the body axis. Development 2001;128:2581–92. [PubMed: 11493574]

Wallingford JB, Rowning BA, Vogeli KM, Rothbächer U, Fraser SE, Harland RM. Dishevelled controls cell polarity during Xenopus gastrulation. Nature 2000;405:81–85. [PubMed: 10811222]

Wallingford JB, Harland RM. Neural tube closure requires Dishevelled-dependent convergent extension of the midline. Development 2002;129:5815–25. [PubMed: 12421719]

Wang F, Kovacs M, Hu A, Limouze J, Harvey EV, Sellers JR. Kinetic mechanism of non-muscle myosin IIB: functional adaptations for tension generation and maintenance. J Biol Chem 2003;278:27439–48. [PubMed: 12704189]

Xu XS, Lee E, Chen T, Kuczmarski E, Chisholm RL, Knecht DA. During multicellular migration, myosin ii serves a structural role independent of its motor function. Dev Biol 2001;232:255–64. [PubMed: 11254362]

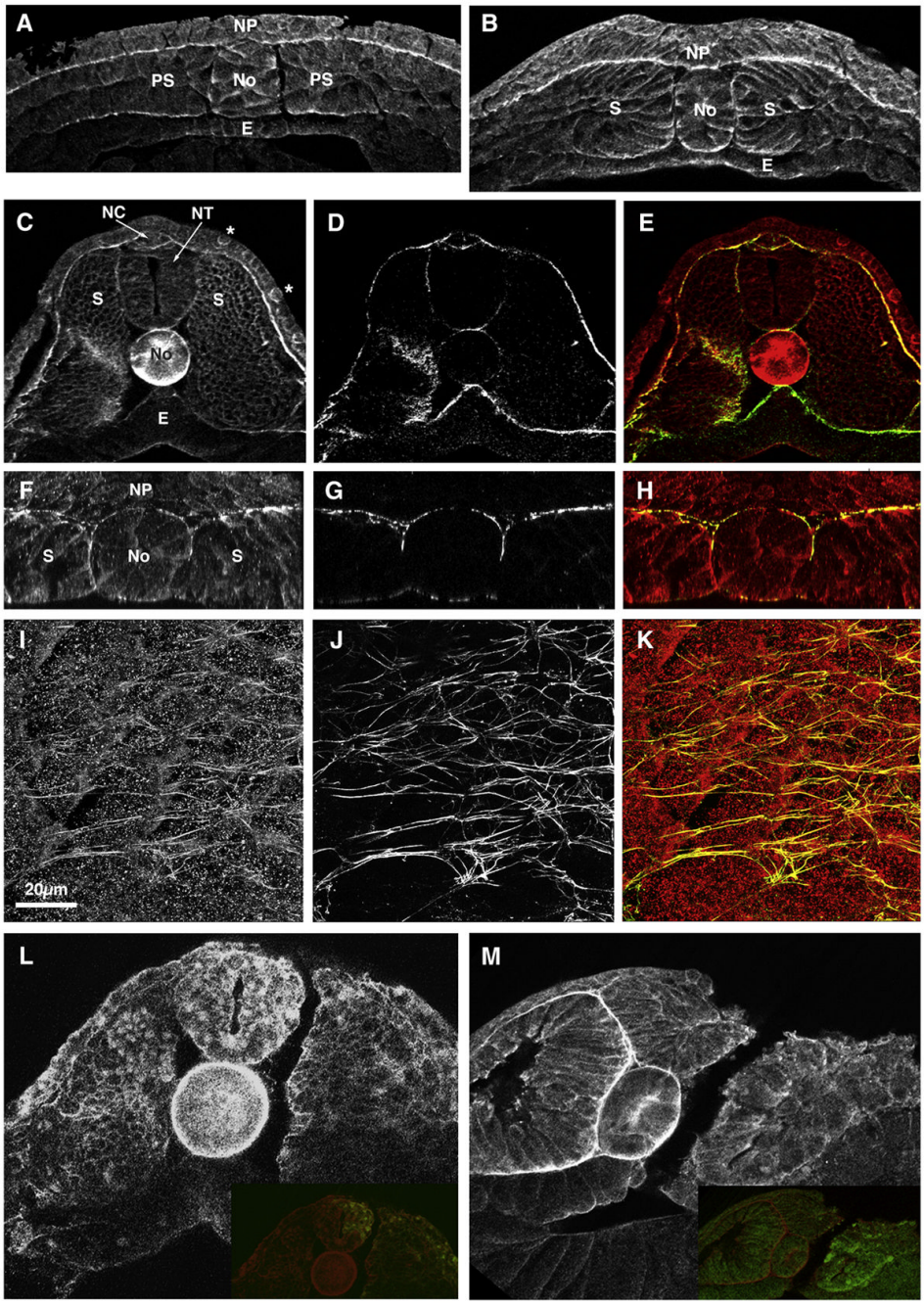

Figure 1. MHC-B expression in the neural plate and its reduction by MHC-B MO

(**A–B**) Transverse sections through the mid-trunk regions of embryos stained for MHC-B at stages 12.5 (**A**) and 16–17 (**B**) show MHC-B on both the deep and the superficial layers of the neural plate (NP), with strongest labeling in the basal ends of deep neural cells. MHC-B is also present in the mesoderm tissues.

(**C–K**) A stage 24 embryo (**C–E**) and a stage 17 neural-deep-over-mesoderm explant (**F–K**) co-stained for MHC-B (**C**, **F**, **I**) and fibronectin (**D**, **G**, **H**), and the respective merged images (**E**, **H**, **K**), coded in red for MHC-B and green for fibronectin are shown.

(**C–D**) A transverse section through the mid-trunk region of a stage 24 embryo shows high MHC-B in the outer basal ends of neural tube (NT) cells, in the neural crest region (NC) and

in the deep layer of the epidermis (**C**), and these areas are coincidental with areas of fibronectin deposition (**D**, **E**). MHC-B levels are very high in the notochord (No) (**C**) (cf. Fig. 2-1) and MHC-B staining is stronger in scattered cells of the outer epidermis (**C**, marked with asterisks *).

(**F–H**) A transverse section through a neural-deep-over-mesoderm explant (obtained by Z-projection of confocal series) shows that, as in whole-embryos, MHC-B is present in the neural and mesoderm tissues, with stronger staining at tissue boundaries (**F**), which coincide with fibronectin localization (**G**, **H**).

(**I–K**) An *en face* view (obtained by XY projections of confocal series) of the boundary between NP and mesoderm in a neural-deep-over-mesoderm explant is shown. Some MHC-B has a fibrilar pattern (**I**) that coincides with fibronectin fibrils (**J**, **K**).

(**L–M**) Transverse sections through the mid-trunk regions of stage 22 embryos injected in one cell at the 2-cell stage with CoMO (**L**) or MHC-B MO (**M**) together with fluorescein-dextran and stained for MHC-B show that MHC-B MO effectively reduces protein levels, whereas CoMO has no discernible effect. Insets are overlapped images of MHC-B staining and fluorescein-dextran lineage label.

NP – neural plate, No – notochord, PS – pre-somitic mesoderm, E – endoderm, S – somitic mesoderm, NT – neural tube, NC – neural crest.

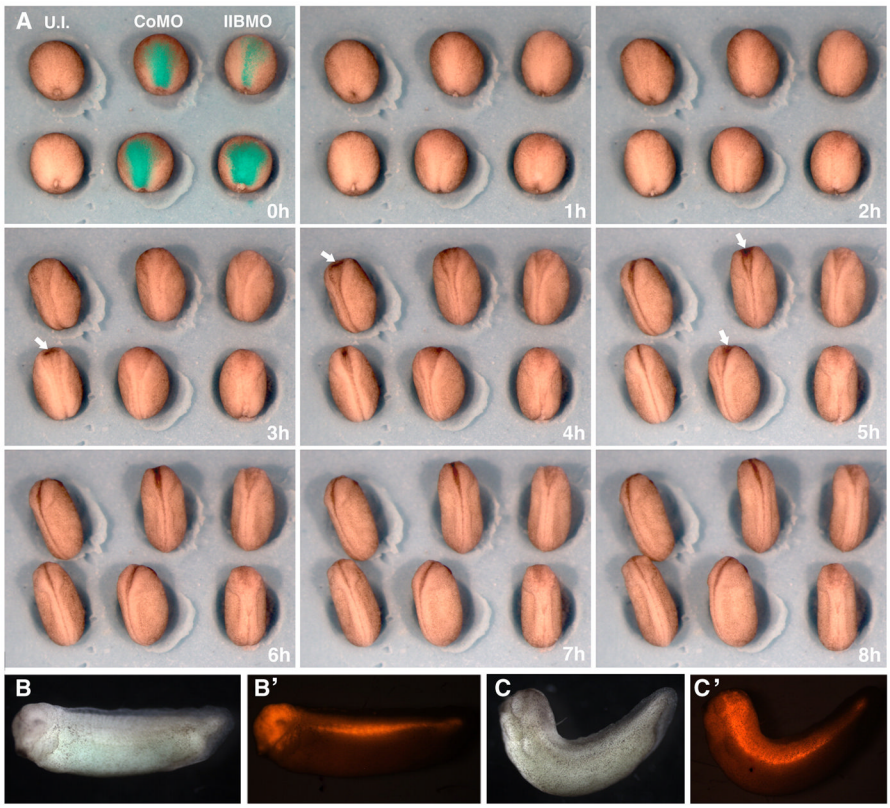

Figure 2. Neural targeted MHC-B MO causes delayed neural tube closure and dorsal flexure of the trunk

(**A**) Time-lapse video-recording frames during neurulation of un-injected embryos and of embryos injected with 2.5μM of either CoMO or MHC-B MO targeted to the neural plated show delayed neural tube closure in MHC-B morphants (dorsal view, anterior is at the top). Rhodamine fluorescence of injected embryos in has been superimposed to the first frame (t=0h), showing successful targeting to the neural plate. The degree of blastopore closure at the onset of neurulation is similar in all three groups, showing that targeting to the mesoderm was avoided. By stages 16/17 (t=3–5h), neural tube closure in MHC-B morphant embryos is delayed throughout the length neural tissue but is more pronounced in the anterior region, where the dark pigmentation of apically constricting bottle cells can be seen in both un-injected and CoMO injected embryos (white arrows), but are never observed in MHC-B morphant embryos. By stage 19/20 (t=8h) the neural tubes have closed in un-injected and CoMO injected embryos, whereas the anterior neural plates remain open in MHC-B MO injected embryos. (**B–C**) Tailbud stage embryos co-injected with either CoMO (**B**) or MHC-B MO (**C**) and rhodamine-dextran targeted to the neural plate (fluorescence can be seen in **B′** and **C′**) show that MHC-B MO causes dorsal flexure of the trunk.

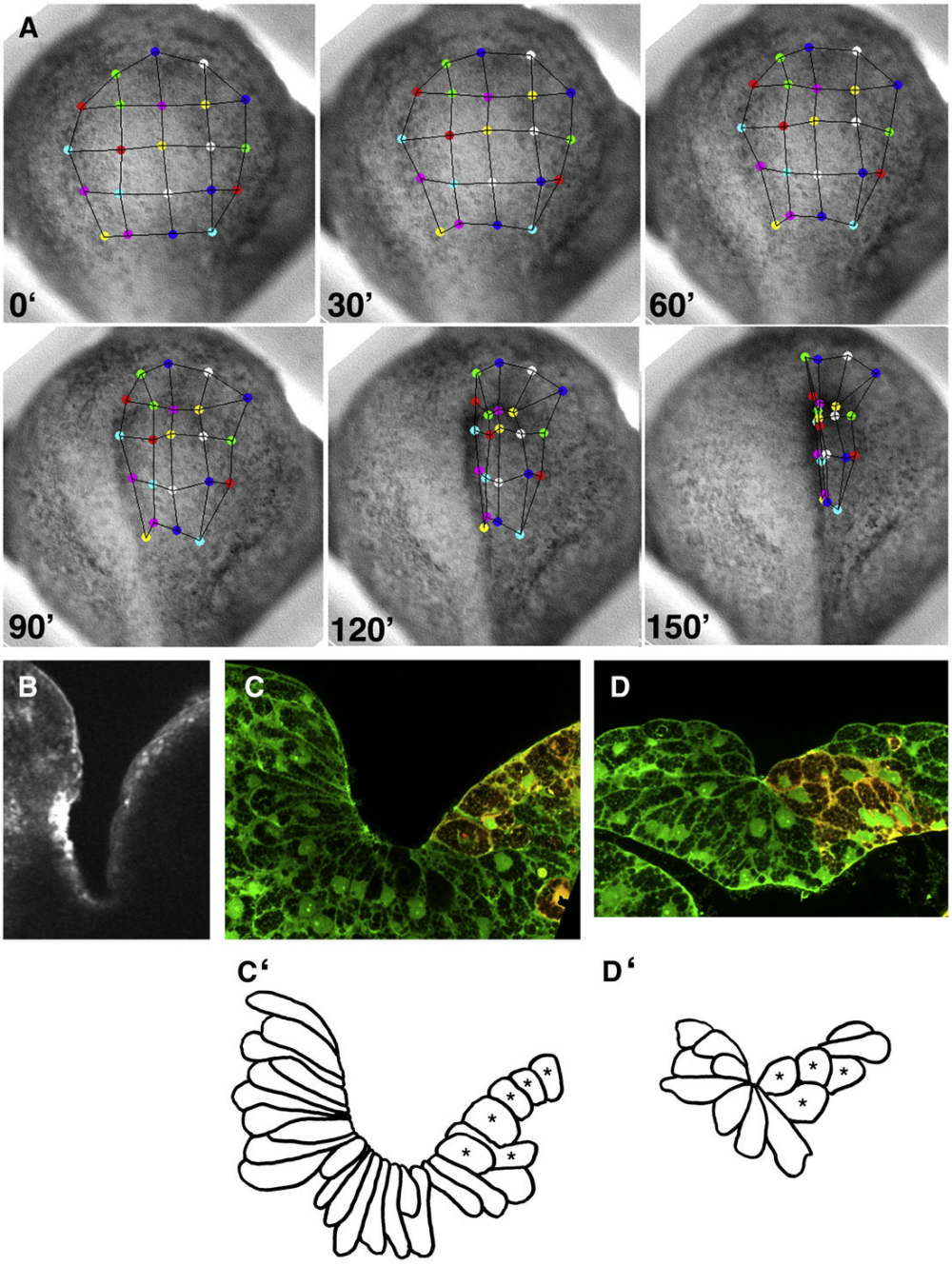

Figure 3. Anterior neural tube closure is asymmetrical in unilaterally neural plate targeted morphants

Movements of colored tracking dots on frames of a time-lapse recording of an anterior view of neural plate (**A**) show that points on the control (left) side move towards the midline faster than points on morphant (right) side of the embryo. A transverse section through the prospective brain region of a stage 18 embryo stained with rhodamine phalloidin (**B**) shows strong apical actin accumulation on the control (left) side, but no actin accumulation on the morphant (right) side. Transverse sections through the prospective brain (**C**) and spinal cord (**D**) regions of a stage 17 embryo show background green fluorescent dextran used to determine cell shape, and red fluorescent dextran co-injected with the MHC-B MO used to identify morphant cells (right

sides). Corresponding tracings of cell outlines (**C′–D′**) show that uninjected cells adopt typical bottle cell morphologies, with long thin necks and constricted apices, whereas morphant cells (*) are short and have broad apices.

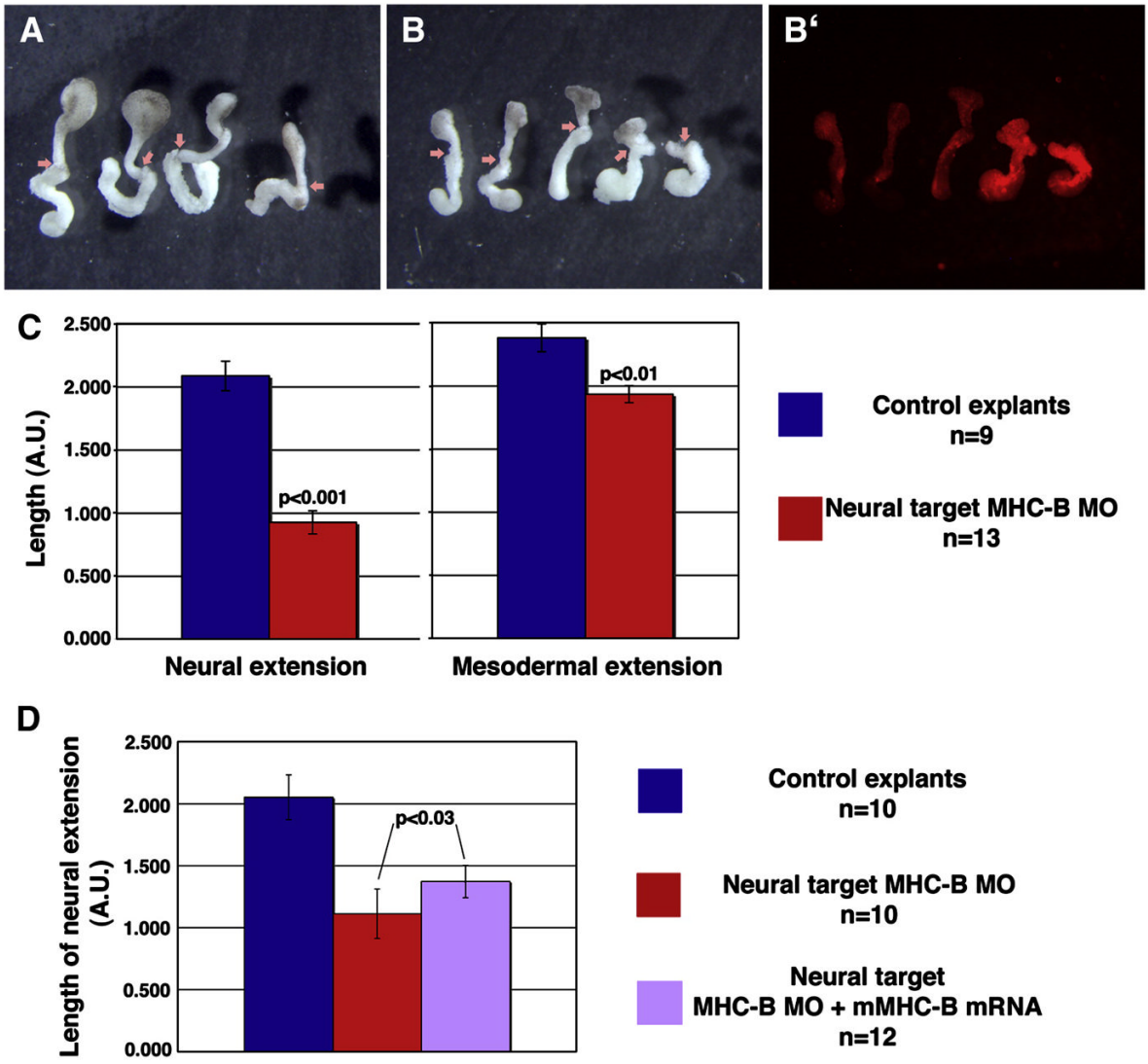

Figure 4. Neural targeted MHC-B MO impairs autonomous neural CE

Keller sandwich explants made from control (**A**) and morphant (**B**) embryos are shown, with arrows indicating the boundaries between neural (top) and mesodermal (bottom) tissues. A fluorescence micrograph (**B′**) shows red fluorescent dextran co-injected with the MO to identify morphant tissues. The extension of neural and mesodermal tissues in control and morphant Keller sandwiches is measured by the final length of tissues in arbitrary units (AU) (**C**). A partial rescue of neural tissue length is achieved by co-injection of MHC-B and mouse MHC-B mRNA (**D**). Error bars are s.e.m., *p*-values were calculated using Student's t-test.

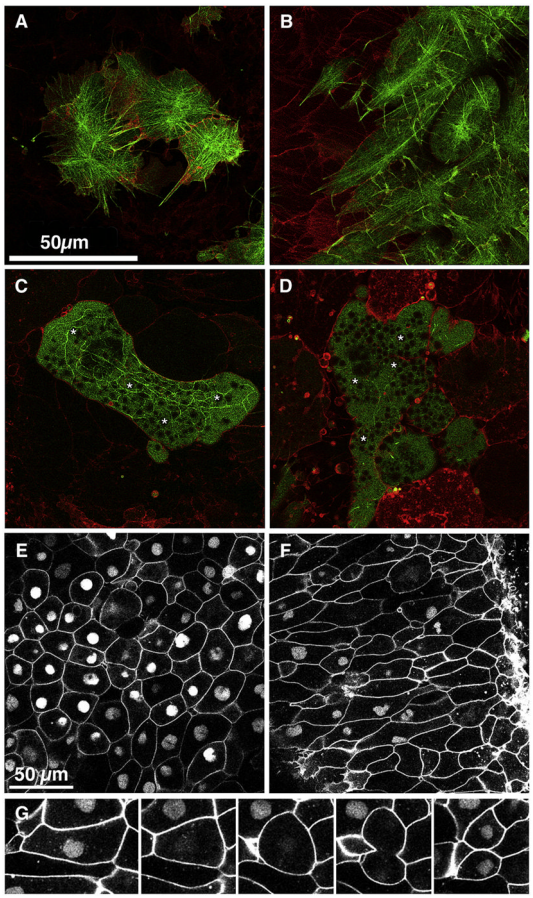

Figure 5. MHC-B reduction causes defects in cell shape and in the cytoskeleton

Laser scanning confocal microscopy shows the cortical regions (<2 μm inside the cytoplasm) of neural deep cells from embryos injected at the two-cell stage with mRNA encoding membrane targeted RFP and at the 32-cell stage with mRNA encoding F-actin targeted GFP alone (**A**) or F-actin targeted GFP with MHC-B MO at 2μM (**B**) or at 2.5μM (**C, D**). Control cells have well-organized cortical network of actin bundles that radiate from foci within the cell (**A**). At 2μM MO, elongated morphant cells have longer actin cables that do not connect foci and they run parallel to direction of elongation (**B**). At 2.5μM MO, morphant cells either have a few coarse, thick actin cables (**C**) or the actin cables are almost absent (**D**). Yolk granules (asterisks * in **C**, **D**) are present in the cortex of cells with higher concentration of MHC-B MO, whereas they are excluded from the cortices of control cells (**A**) and low-dose morphant cells (**B**). Neural deep cells from embryos injected at the two-cell stage with mRNAs encoding membrane-targeted GFP and at the 32-cell stage with nuclear-targeted GFP (NLS-GFP) alone (**E**) or NLS- GFP and MHC-B MO (**F**) are shown. Morphant cells (having nuclear GFP in **F**) are more elongated than control cells (**E**). Frames from a time-lapse video-recording (**G**) show a cell undergoing mitosis and cytokinesis. This cell is initially elongated (0′), and it rounds up to undergo cell division (33′). The NLS-GFP becomes invisible upon nuclear envelope breakdown (23′) and reappears after cytokinesis and re-formation of nuclei in the daughter cells (58′). The scale bar in **A** applies to **B–D**. Scale bar in **E** applies to **F**.

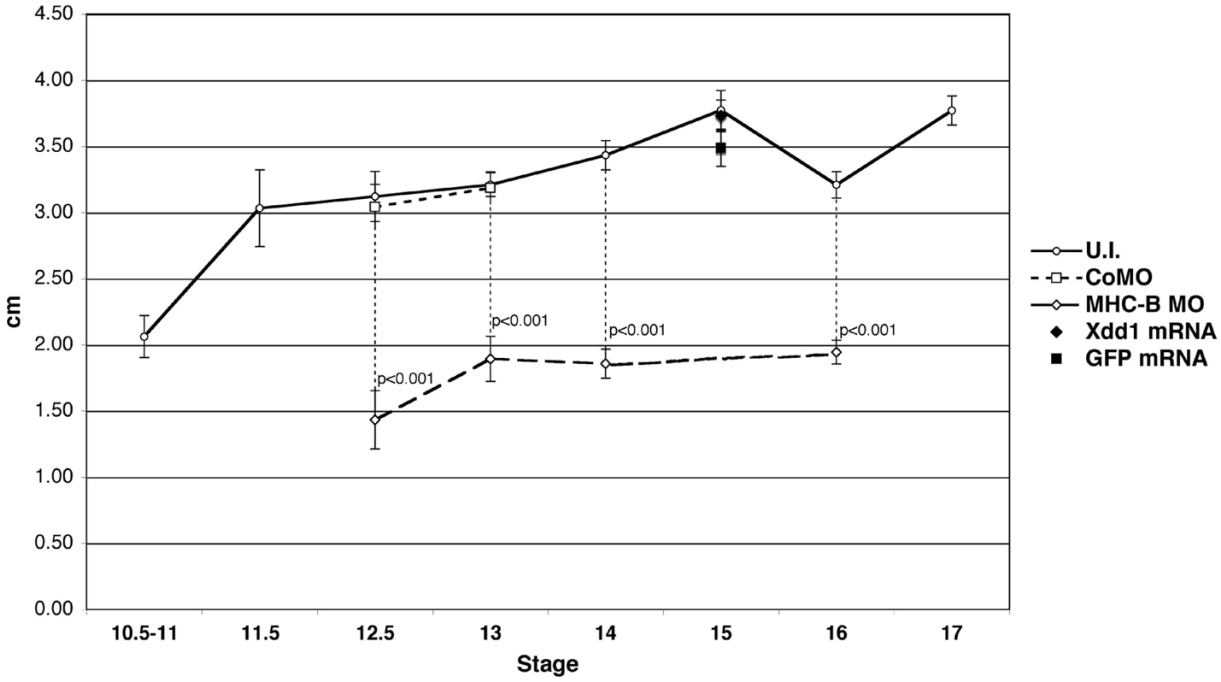

Figure 6. MHC-B MO increases deformability of the neural plate

Measurements of negative pressure (expressed as height of a water column in cm) required to produce a bulge of a fixed size in the neural plate using an elastimeter are plotted across different developmental stages. The amount of negative pressure in un-injected embryos increases throughout development, showing that these become increasingly resistant to deformation. MHC-B morphant neural plates are significantly more pliable than wild-type ones, whereas CoMO embryos are similar to controls. Neural plates injected with mRNA encoding for Xdd1 or GFP show no difference in deformability, either compared to one another or compared to un-injected embryos. Error bars are s.e.m., *p*-values were calculated using Student's t-test.